Differentiable Thermo-Solutal Drift-Flux Inference for Real-Time Gas-Kick Detection Under Uncertainty

Apichai Srisuwan[1], Nattapon Kanchana[2], and Worawit Chaiyasit[3]
[1]Chiang Rai Rajabhat University, 80 Moo 9, Phahonyothin Road, Ban Du, Chiang Rai 57100, Thailand
[2]Roi Et Rajabhat University, 59 Moo 11, Roi Et–Selaphum Road, Roi Et 45120, Thailand
[3]Nakhon Phanom University, 103 Moo 3, Nakhon Phanom–That Phanom Road, Nakhon Phanom 48000, Thailand

ABSTRACT Transient gas influx into a drilling annulus remains a principal source of operational risk because small early-stage perturbations can evolve into rapid gas unloading at the surface. Conventional monitoring relies on sparse, noisy surface signals whose relationship to downhole multiphase dynamics is strongly nonlinear and history dependent through compressibility, slip, and thermodynamic exchange between phases. This paper develops a real-time, physics-constrained inference framework that couples a thermo-hydrodynamic drift-flux model with a solubility-consistent thermodynamic closure, yielding a differentiable simulator suitable for online inversion. The central contribution is a state-space formulation in which gas influx is treated as an unknown, time-varying boundary flux and estimated jointly with uncertain hydraulic and mass-transfer parameters from pit-volume, pump-rate, and wellhead-pressure observations. Differentiability is enforced by implicit solvers and adjoint sensitivity methods, enabling fast gradient-based posterior updates and likelihood-ratio detection statistics. The model incorporates a unified representation of free-gas holdup, dissolved-gas inventory, and energy transport so that delays induced by dissolution and thermal expansion can be separated from hydraulic signatures. Numerical experiments demonstrate stable online estimation across regimes spanning non-circulating to high-rate circulation, with detection latency governed by observability limits rather than solver cost. The framework is intended as a computational backbone for kick-aware automation, emphasizing uncertainty quantification and identifiability over scenario-specific tuning.

KEYWORDS

1. Introduction

Gas influx during drilling operations perturbs the coupled hydraulic, thermal, and compositional state of the wellbore and riser [1]. The operational difficulty is not merely that gas is hazardous, but that the earliest signatures of influx can be statistically indistinguishable from benign transients caused by pump ramps, heave, temperature drift, cuttings loading, and sensor bias. The physical system amplifies modeling errors: compressible gas introduces strong nonlinearity in the pressure–volume relation; slip between phases breaks the direct link between mixture flow and gas migration; and dissolution into non-aqueous drilling fluids can temporarily conceal gas mass while altering effective mud properties and delaying surface indicators. As a result, the problem of early kick detection is fundamentally an inverse problem under partial observability, where one seeks to infer an unmeasured downhole influx from limited measurements through a model that is itself uncertain [2].

A recurring theme in the technical literature is that many detection schemes are built on low-order heuristics, while mechanistic simulators can be too slow or too calibration dependent for continuous field use. A broad review of transient multiphase-flow approaches highlights that most published early-detection models are one-dimensional and only partially incorporate heat transfer and solubility, and it argues that richer multidimensional descriptions could improve the fidelity of velocity, temperature, and pressure fields relevant to detection performance [3]. At the same time, increasing model fidelity alone does not resolve the real-time inverse problem: richer models are typically more computationally expensive and introduce additional uncertain

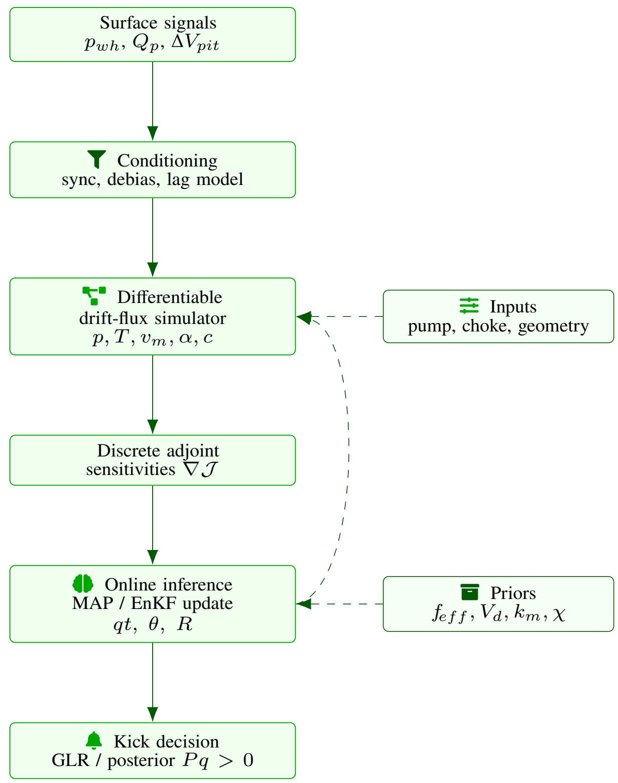

Figure 1 End-to-end real-time kick inference loop: conditioned surface measurements drive a differentiable thermo-solutal drift-flux model; discrete-adjoint sensitivities enable fast online updates of influx history qt and uncertain closures θ, producing probabilistic detection statistics and actionable alerts.

closures that can degrade identifiability when data are sparse. The practical requirement is therefore not maximal physical detail, but a model class that is sufficiently expressive to map influx to surface observables while remaining computationally tractable and statistically well posed when embedded in an estimator.

This paper advances a framework that is deliberately positioned between heuristic monitoring and large-scale computational fluid dynamics [4]. The proposed approach starts from a drift-flux representation of annular gas–liquid transport augmented with energy and dissolution inventory, but it is re-engineered to be differentiable with respect to both state and parameters. Differentiability is not an aesthetic preference; it is a structural enabler for modern estimation. In a Bayesian or regularized maximum-likelihood setting, the estimator requires repeated evaluation of gradients of the measurement misfit with respect to influx and uncertain parameters. If those gradients are computed through finite differences, the computational burden scales poorly with parameter dimension and becomes brittle under solver noise [5]. If instead gradients are computed through an adjoint of the fully implicit time integrator, then the marginal cost of high-dimensional inference can be reduced to a small multiple of one forward simulation, bringing online inversion within reach.

The technical thesis of this work is that a properly constrained, differentiable, thermo-solutal drift-flux model can serve as the core of a real-time kick detection and characterization engine. The contribution is not a new empirical correlation, nor a mere synthesis of prior kick simulators, but a modeling-and-inference architecture that (i) treats influx as a time-distributed control to be inferred, (ii) maintains thermodynamic consistency between free and dissolved gas so that dissolution-induced delays are modeled rather than absorbed into bias, and (iii) exposes stable sensitivities through implicit discretization and adjoint methods so that online estimation can be performed under uncertainty. The framework is designed to support two operational questions that are often conflated but should be separated: whether an influx is occurring (detection), and what its magnitude and timing are (characterization) [6]. By formulating both as probabilistic inference, the method produces not only point estimates but also uncertainty bands that can be mapped into decision thresholds.

The remainder of the paper introduces the governing equations and closures in a form suitable for inference, derives the inverse problem and detection statistics, and discusses numerical implementation choices needed to ensure robustness under the stiffness typical of gas expansion and dissolution kinetics. Throughout, the emphasis is on mechanisms that influence observability of a kick from surface data, rather than on reproducing any single benchmark scenario.

2. Thermo-Hydrodynamic Formulation for Annular Kick Transients

Consider a wellbore or riser annulus of length L parameterized by measured depth $z \in 0, L$, with $z = 0$ at the surface and

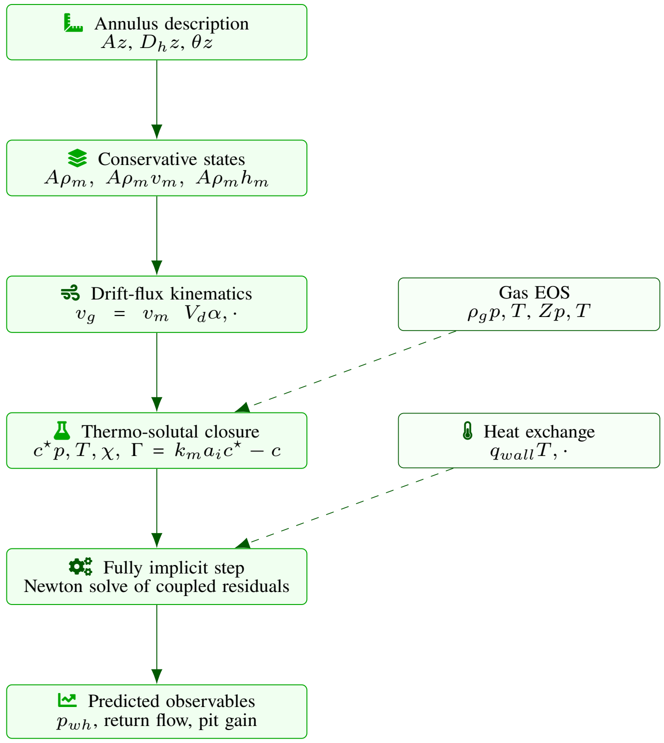

Figure 2 Compact decomposition of the thermo-hydrodynamic drift-flux core: conservative transport variables are evolved with drift-flux kinematics and smooth thermo-solutal closures (equilibrium $c^\star$ and finite-rate transfer Γ), solved via a coupled implicit step to produce surface-facing predictions used by the estimator.

$z = L$ at the influx location (or at the bottom boundary of the modeled domain) [7]. The annulus cross-sectional area is Az and hydraulic diameter is $D_h z$, allowing tapered geometries. The flow is modeled as a one-dimensional, two-phase mixture with a liquid drilling fluid and a gas phase that may be present as free bubbles and as dissolved mass in the liquid. The state variables are chosen to balance physical expressiveness with estimator stability: mixture pressure pz, t, mixture velocity $v_m z, t$, temperature Tz, t, free-gas volume fraction $\alpha z, t$, and a dissolved-gas mass fraction (or concentration) cz, t defined per unit liquid mass. The free gas density is $\rho_g p, T$ and the liquid density is $\rho_l p, T, c$, with ρ_l allowed to depend weakly on dissolved gas through swelling [8].

A convenient starting point is the conservation of total mass, augmented by a separate conservation of gas mass partitioned between free and dissolved inventories. Define the mixture density $\rho_m = \alpha\rho_g \ 1 - \alpha\rho_l$ and the liquid superficial velocity v_l and gas velocity v_g. With drift-flux kinematics, the phase velocities are written in terms of the mixture velocity v_m and a slip relation. The volumetric flux is $j = v_m$, and the drift-flux closure takes the form [9]

$$
\begin{aligned}
v_g &= v_m \ \ V_d \alpha, p, T, \mathcal{G}, \\
v_l &= v_m - \frac{\alpha}{1-\alpha} V_d \alpha, p, T, \mathcal{G}, \\
\mathcal{G} &= \{A, D_h, \theta\}.
\end{aligned} \tag{2.1}
$$

where θz is inclination and V_d is a drift velocity that captures buoyant rise relative to the mixture. The dependence on geometry $\mathcal{G}$ is explicit because annular slip differs from pipe slip and because inclination modifies buoyancy projections.

The conservation of total mass for the two-phase mixture can be expressed as

$$
\frac{\partial}{\partial t}\left(A\rho_m\right) \ \frac{\partial}{\partial z}\left(A\rho_m v_m\right) = 0, \tag{2.2}
$$

which is exact when no net mass enters or leaves the modeled domain aside from boundary fluxes. Gas mass conservation is more informative when split into free and dissolved parts [10]. Let $m_{gd} = A1 - \alpha\rho_l c$ denote dissolved-gas mass per unit length and $m_{gf} = A\alpha\rho_g$ denote free-gas mass per unit length. Interphase mass transfer $\Gamma z, t$ converts between these inventories without changing total mass. Then

$$
\frac{\partial}{\partial t}\left(A\alpha\rho_g\right) \ \frac{\partial}{\partial z}\left(A\alpha\rho_g v_g\right) = -A\Gamma \ \ As_g, \tag{2.3}
$$

$$
\frac{\partial}{\partial t}\left(A1 - \alpha\rho_l c\right) \ \frac{\partial}{\partial z}\left(A1 - \alpha\rho_l c\, v_l\right) = A\Gamma, \tag{2.4}
$$

where s_g is an optional source term representing distributed gas entry (typically $s_g = 0$ in the interior and the influx is imposed as a boundary condition at $z = L$). The sign convention is such that $\Gamma > 0$ corresponds to dissolution (free gas transferring into the liquid), while $\Gamma < 0$ corresponds to exsolution.

Momentum is modeled at the mixture level to avoid the stiffness of separate phase momentum under sparse measurement constraints [11]. A compressible mixture momentum balance

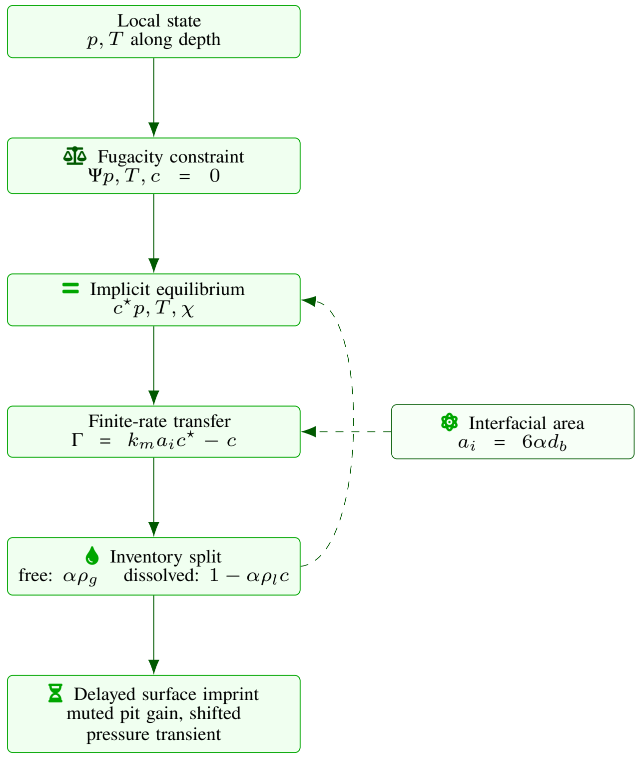

Figure 3 Solubility-consistent partitioning of gas mass: an implicit equilibrium condition defines $c^{\star}p, T, \chi$, while finite-rate transfer Γ exchanges mass between dissolved and free inventories, producing characteristic delays and smoothing in surface observables that can be disentangled during inference.

with wall friction and gravity is written as

$$\frac{\partial}{\partial t}\left(A\rho_m v_m\right)\ \frac{\partial}{\partial z}\left(A\rho_m v_m^2\right)\ A\frac{\partial p}{\partial z} = -A\rho_m g\cos\theta - A\Delta_w, \tag{2.5}$$

where Δ_w is the wall shear contribution expressed per unit volume. For annular flow, Δ_w is typically modeled as a function of an effective friction factor and the mixture Reynolds number, but for inference the closure must be smooth and differentiable. A representative differentiable form is [12]

$$\Delta_w = \frac{2f_{\text{eff}}\text{Re}_m, \alpha\rho_m v_m|v_m|}{D_h}, \quad \text{Re}_m = \frac{\rho_m|v_m|D_h}{\mu_{\text{eff}}\alpha, T, \gamma}, \tag{2.6}$$

with μ_{eff} an effective viscosity that can approximate non-Newtonian behavior through a differentiable surrogate in terms of shear rate γ inferred from v_m and geometry.

Thermal effects are incorporated because gas expansion, density, and solubility are temperature dependent and because circulation modifies the thermal boundary layer. A pragmatic energy balance uses a single mixture temperature with interfacial equilibrium assumed rapid relative to axial transport. Let $h_m\alpha, p, T, c$ denote mixture specific enthalpy. Then

$$\frac{\partial}{\partial t}\left(A\rho_m h_m\right)\ \frac{\partial}{\partial z}\left(A\rho_m v_m h_m\right) = -Av_m\frac{\partial p}{\partial z}\ Aq_{\text{wall}}\ Aq_{\text{rxn}}, \tag{2.7}$$

where q_{wall} is net heat exchange with formation or seawater across the annulus boundary, and q_{rxn} can represent latent effects associated with dissolution/exsolution if desired. In many drilling applications, dissolution heat is small relative to hydraulic work and wall heat transfer, but including it as a parameterized term can improve identifiability when temperature data are available [13].

The above equations become predictive only when closed by constitutive relations for ρ_g, ρ_l, h_m, V_d, and Γ. While a variety of closures exist, this work requires that closures be continuously differentiable and numerically stable under implicit discretization. For gas density, an equation of state provides $\rho_g p, T$ with compressibility. For the liquid, a slightly compressible relation suffices provided it permits swelling with dissolved gas through a volumetric factor embedded in $\rho_l p, T, c$ [14]. For slip, V_d is selected to recover the correct limits: $V_d \to 0$ as $\alpha \to 0$ (no resolved bubbles) and V_d bounded as $\alpha \to 1$ (gas-dominated). A robust choice is a buoyancy-driven form modulated by a hindrance function $H\alpha$ and an annular hydraulic scaling:

$$V_d = H\alpha\sqrt{\frac{gD_h\cos\theta}{C_d}}\ \phi\text{Eo}, \text{Mo}, \quad H\alpha = \left(1-\alpha\right)^{n_h}, \tag{2.8}$$

where C_d and n_h are closure parameters, and ϕ captures bubble-shape effects through dimensionless groups. In inference, C_d and n_h can be treated as uncertain but bounded, with priors centered on values consistent with annular bubbly flow [15].

An important modeling decision is how to represent dissolution. Many operational simulators either neglect solubility or

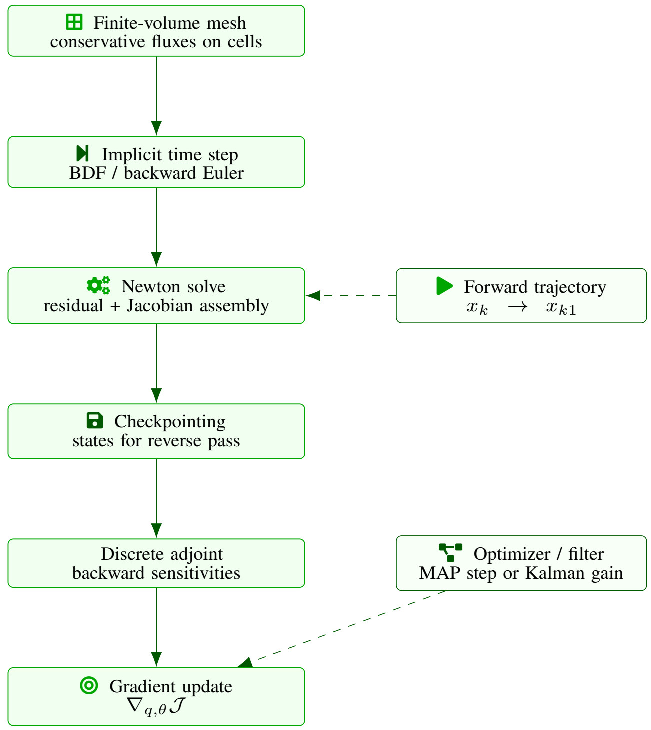

Figure 4 Numerical pathway enabling real-time inversion: conservative finite-volume discretization and implicit stepping provide stiffness robustness, while consistent discrete-adjoint propagation (supported by checkpointing) delivers stable gradients for high-dimensional influx and parameter updates.

treat it through ad hoc delay factors, which can bias detection logic when synthetic or oil-based muds are used. State-of-the-art semi-analytical annular kick modeling that explicitly represents gas solubility in non-aqueous drilling fluids and its impact on ascent time and surface indicators has been reported in [16], including scenarios where dissolution lengthens the time for gas to reach the wellhead relative to insoluble assumptions. The framework developed here does not replicate that simulator; instead it embeds solubility into a differentiable state representation so that dissolution becomes an estimable mechanism in the inverse problem rather than a fixed scenario assumption. This distinction is critical for online detection because the estimator must be able to explain delayed or muted surface signals either as reduced influx or as enhanced dissolution capacity, and it must do so with quantified uncertainty [17].

Boundary conditions couple the downhole and surface operational controls to the PDE system. At the surface, pressure is tied to choke and separator conditions; at the bottom, the influx is represented as an unknown gas mass flux (and potentially a liquid flux) entering the annulus. For example, at $z = L$ one can impose

$$A\alpha\rho_g v_g|_{z=L} = m_{\text{in}}t, \quad A\rho_m v_m|_{z=L} = m_{\text{circ}}t\ m_{\text{in}}t, \tag{2.9}$$

where $m_{\text{circ}}t$ is the imposed circulation mass flow rate and $m_{\text{in}}t$ is the unknown influx to be inferred. The observational model, introduced later, maps the evolving state to wellhead pressure and pit volume change, with pit gain linked to net surface-return flow and density [18].

3. Solubility-Constrained State Variables and Thermodynamic Closure

To separate hydraulic transients from compositional hiding of gas mass, the model must represent the partitioning of methane (or a generic hydrocarbon gas) between a free phase and dissolved inventory. The key requirement is consistency: dissolved gas cannot be treated as an independent scalar divorced from pressure and temperature, because at sufficiently low pressure or high temperature the fluid exsolves and produces free gas even without additional influx. Conversely, at high pressure and moderate temperature, a significant fraction of the influx may remain dissolved, reducing free-gas holdup and muting surface indicators. From an estimation standpoint, this coupling is both a challenge and an opportunity: it complicates the map from influx to measurements, but it also introduces distinctive signatures, such as delayed gas appearance and modified compressibility, that can improve identifiability when modeled explicitly [19].

The closure adopted here uses a constrained-equilibrium representation augmented by finite-rate transfer. Define a local equilibrium dissolved concentration $c^\star p, T, \chi$ where χ collects liquid composition parameters associated with the drilling fluid base oil and additives. In a synthetic or oil-based mud, $c^\star$ is typically much larger than in water-based mud, and it is strongly pressure dependent. Rather than relying on an empirical solubility curve that may be outside its calibration range, the framework treats $c^\star$ as the solution of an implicit thermodynamic condition expressed in terms of fugacities [20]. Let $f_g p, T$ denote gas-phase fugacity and $f_l p, T, c$ denote the fugacity of

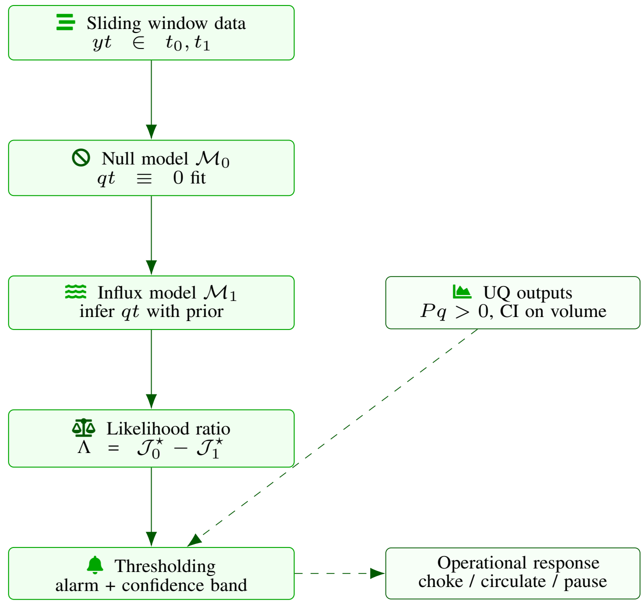

Figure 5 Online detection framing as model comparison: a null (no-influx) fit is contrasted with an inferred-influx fit over a short window, yielding a likelihood-ratio statistic and uncertainty-aware decision outputs that support threshold-based alarms and graded responses.

the dissolved gas in the liquid mixture. Local equilibrium is defined by

$$\Psi p, T, c = \ln f_g p, T - \ln f_l p, T, c = 0,$$
$$c^\star p, T, \chi \text{ solves } \Psi p, T, c^\star = 0. \tag{3.1}$$

This formulation is advantageous for differentiability because $c^\star$ can be differentiated with respect to p, T via the implicit function theorem:

$$\frac{\partial c^\star}{\partial p} = -\frac{\partial \Psi \partial p}{\partial \Psi \partial c}\Big|_{c=c^\star}, \quad \frac{\partial c^\star}{\partial T} = -\frac{\partial \Psi \partial T}{\partial \Psi \partial c}\Big|_{c=c^\star}. \tag{3.2}$$

In practice, f_g can be computed from an equation of state through a fugacity coefficient, while f_l can be computed from an activity-coefficient or EOS-based liquid model [21]. The details of these thermodynamic models vary across mud systems; for the present purpose, the estimator requires only that Ψ be smooth, monotone in c near equilibrium, and evaluable with stable derivatives. The parameters χ can be treated as calibration parameters representing effective solubility capacity rather than exact chemical composition.

Equilibrium alone is insufficient because dissolution and exsolution occur on finite time scales determined by bubble surface area, turbulence, and mass-transfer coefficients. Therefore, the interphase transfer rate Γ is modeled as a relaxation toward equilibrium in concentration space, modulated by interfacial area density [22]. A differentiable, physically interpretable form is

$$\Gamma = k_m a_i \left(c^\star p, T, \chi - c\right), \quad a_i = \frac{6\alpha}{d_b \alpha, p, T}, \tag{3.3}$$

where k_m is a mass-transfer coefficient, a_i is interfacial area per mixture volume, and d_b is an effective bubble diameter that may depend on flow regime and can be parameterized smoothly. This closure ensures that when $c < c^\star$, dissolution occurs ($\Gamma > 0$), reducing free gas; when $c > c^\star$, exsolution occurs ($\Gamma < 0$), generating free gas. Importantly, the closure automatically links dissolution dynamics to holdup through a_i, creating a feedback: higher holdup increases interfacial area and accelerates equilibration, while low holdup slows mass exchange [23].

The drilling fluid density and enthalpy require consistent dependence on dissolved gas. For many muds, swelling due to dissolved gas affects the effective liquid formation volume and thereby changes hydrostatic and frictional terms. A minimal yet consistent approach uses a liquid specific volume $v_l^{\text{spec}} p, T, c$ expanded around a reference state:

$$v_l^{\text{spec}} p, T, c = v_{l,0}\left(1 \;\; \beta_T T - T_0 - \beta_p p - p_0 \;\; \beta_c c - c_0\right),$$
$$\rho_l = \left(v_l^{\text{spec}}\right)^{-1}. \tag{3.4}$$

with $\beta_T, \beta_p, \beta_c$ treated as uncertain but bounded coefficients. This representation is not intended to replace detailed PVT modeling; its role is to capture first-order coupling between dissolution and hydraulics in a way that can be inferred from pressure and pit-gain signals [24]. The energy model uses compatible expansions for enthalpy to maintain thermodynamic plausibility.

A notable operational regime is synthetic-based mud in deepwater risers, where methane dissolution can be substantial over large depths and pressures, and gas may remain largely dissolved until it approaches shallower, lower-pressure segments. A mechanistic riser model that analytically predicts key kick parameters and explicitly models methane solubility in synthetic-based drilling fluids, including validation against a process-simulation tool and experimental flow-loop observations, has been presented in [25], representing a state-of-the-art treatment of methane dissolution for this application. The present work

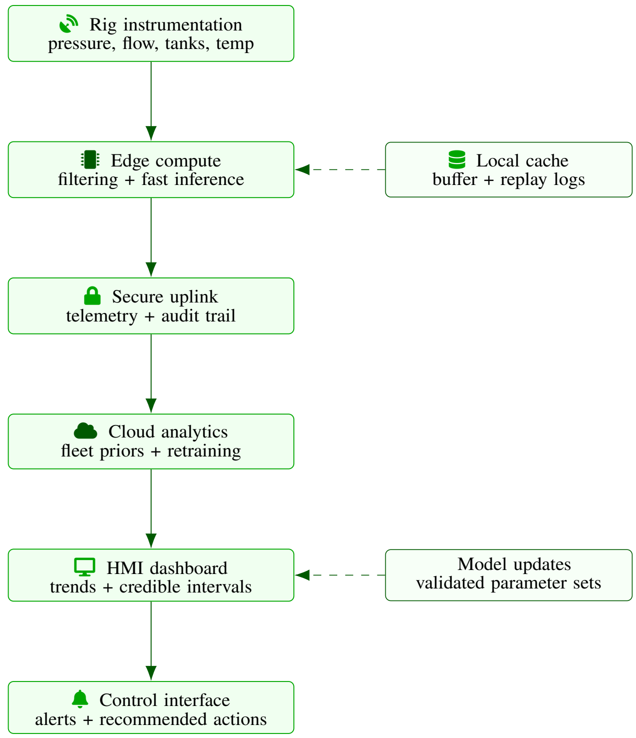

Figure 6 Deployment-oriented architecture: low-latency edge inference consumes rig telemetry and issues uncertainty-aware alerts, while secure connectivity supports logging, fleet-level analytics, and validated model updates without interrupting real-time operation.

leverages the conceptual importance of such thermodynamic consistency but repositions it within a differentiable inference engine: solubility is not merely predicted forward; it is embedded as a constrained latent mechanism whose parameters can be updated online to reconcile model and measurements under uncertainty.

From the standpoint of identifiability, dissolution introduces a structured ambiguity: a given reduction in observed pit gain could be explained either by a smaller influx or by a larger fraction of influx being stored in the dissolved inventory [26]. This ambiguity can be mitigated by multi-sensor fusion. Temperature data, if available, constrains $c^\star$ through its temperature dependence. Likewise, transient pressure signatures constrain free-gas compressibility and thus holdup evolution. The model is constructed so that these constraints enter smoothly through the thermodynamic closure, allowing a probabilistic estimator to propagate uncertainty rather than forcing a single deterministic interpretation [27].

The final closure element is the mapping from dissolved concentration to gas-phase appearance. In the PDE system, free gas holdup α evolves through the free-gas mass balance; if exsolution occurs, $\Gamma < 0$ increases free gas mass, but the conversion from mass to volume depends on $\rho_g p, T$ and thus on pressure. This can create stiff behavior near bubble-point-like conditions, where small pressure changes generate large volume changes [28]. To address stiffness while preserving differentiability, the solver uses implicit time stepping with a Newton method that treats p, α, c, T, v_m as coupled unknowns and computes consistent Jacobians. This is essential for stable sensitivities, because the estimator relies on gradients that would otherwise be corrupted by solver nonconvergence or discontinuous phase appearance logic.

4. Inverse Problem and Real-Time Bayesian Detection

The physical model defines a nonlinear operator mapping unknown influx and parameters to surface observables. Early kick detection requires inverting that map online [29]. Let xt denote the discretized state vector representing fields p, T, v_m, α, c over depth, and let ut denote known operational inputs such as pump rate, choke setting, and mud properties measured at surface. Let θ denote uncertain but slowly varying parameters, including effective friction and slip parameters, heat-transfer coefficients, solubility-capacity parameters χ, and mass-transfer coefficients. The unknown influx is represented as a time-varying boundary flux qt (mass or standard-volume rate) at the bottom boundary. After spatial discretization, the PDE system becomes a differential-algebraic system of the form [30]

$$M x, \theta x = F x, u, q, \theta, \quad y = H x, u, \theta\ \varepsilon, \tag{4.1}$$

where M is a mass matrix arising from conservative discretization, F encodes fluxes and sources, and yt denotes observations such as wellhead pressure, standpipe pressure, return flow rate, and pit volume. The noise term ε aggregates sensor noise, unmodeled dynamics, and discretization residuals; it is modeled as Gaussian with covariance R for tractability, acknowledging that heavier tails can be incorporated if needed.

The inference task is to estimate qt and θ from streaming observations. A direct approach is maximum a posteriori

Symbol	Description	Units	Notes
pz, t	Mixture pressure	Pa	Drives compressibility and solubility
Tz, t	Mixture temperature	K	Affects density, solubility, EOS
$v_m z, t$	Mixture velocity	m/s	Defines volumetric flux $j = v_m$
$\alpha z, t$	Free-gas volume fraction	–	Controls holdup and slip
cz, t	Dissolved-gas mass fraction (per liquid mass)	kg/kg	Thermodynamic partitioning variable
ρ_m	Mixture density $\rho_m = \alpha\rho_g \; 1 - \alpha\rho_l$	kg/m^3	Appears in all conservative balances
xt	Discretized state vector $\{p, T, v_m, \alpha, c\}$	–	State in inverse problem formulation

Table 1 Core state variables in the thermo-solutal drift-flux formulation for annular gas–liquid transients.

Quantity	Conservative variable	Schematic balance	Eq.
Total mass	$A\rho_m$	$\partial_t A\rho_m \; \partial_z A\rho_m v_m = 0$	(2)
Free-gas mass	$A\alpha\rho_g$	$\partial_t A\alpha\rho_g \; \partial_z A\alpha\rho_g v_g = -A\Gamma \; As_g$	(3)
Dissolved-gas mass	$A1 - \alpha\rho_l c$	$\partial_t A1 - \alpha\rho_l c \; \partial_z A1 - \alpha\rho_l c v_l = A\Gamma$	(4)
Mixture momentum	$A\rho_m v_m$	$\partial_t A\rho_m v_m \; \partial_z A\rho_m v_m^2 \; A\,\partial_z p = -A\rho_m g\cos\theta - A\Delta_w$	(5)
Energy	$A\rho_m h_m$	$\partial_t A\rho_m h_m \; \partial_z A\rho_m v_m h_m = -Av_m\partial_z p \; Aq_{\text{wall}} \; Aq_{\text{rxn}}$	(6)

Table 2 Summary of conservative balances used in the annular thermo-hydrodynamic formulation. Equation labels are indicative of the forms introduced in the text.

estimation in a moving time window [31]. Over a window $t \in t_0, t_1$, define the negative log posterior functional

$$\mathcal{J}q, \theta = \frac{1}{2}{}_{t_0}^{t_1} \left(yt - Hxt, ut, \theta\right)^{\mathsf{T}} R^{-1} \left(yt - Hxt, ut, \theta\right) \, dt \quad \frac{1}{2}\left(\theta - \theta_0\right)^{\mathsf{T}} P^{-1} \left(\theta - \theta_0\right) \; \frac{\lambda}{2}{}_{t_0}^{t_1} \left(\frac{d^2 q}{dt^2}\right)^2 dt, \tag{4.2}$$

subject to the dynamics $Mx = F$ and boundary conditions. The prior mean θ_0 and covariance P encode engineering knowledge about plausible parameter ranges. The regularization on q penalizes unrealistically oscillatory influx and functions as a prior on influx smoothness; the second-derivative penalty favors piecewise-smooth influx consistent with reservoir-driven entry rather than measurement noise. Alternative priors can be imposed, such as sparsity-promoting penalties if the goal is to detect brief influx events, but smoothness is a reasonable default for drilling transients [32].

To solve this constrained optimization online, the method uses an adjoint formulation. Let $Gx, q, \theta = Mx, \theta x - Fx, u, q, \theta = 0$ denote the discretized dynamics. Introduce a Lagrange multiplier $\lambda_x t$ and define an augmented Lagrangian whose stationarity yields the adjoint equations. For implicit time integrators, it is convenient to derive discrete adjoints consistent with the time-stepping scheme so that gradients reflect the actual numerical trajectory rather than the continuous idealization. The key outcome is that the gradient of $\mathcal{J}$ with respect to high-dimensional qt can be computed at cost proportional to one backward adjoint solve, independent of the dimension of q after time discretization. This property is what enables treating influx as a function rather than as a low-dimensional parameterization [33].

In addition to point estimation, detection requires deciding whether qt is nonzero in a statistically meaningful sense. This is formulated as a model comparison problem between a null model $\mathcal{M}_0$ in which $qt \equiv 0$ and an alternative model $\mathcal{M}_1$ in which qt is inferred. A practical online statistic is a generalized

Parameter	Role in drift-flux closure	Prior mean	Prior range
C_d	Drag coefficient in V_d scaling $\sqrt{gD_h \cos\theta C_d}$	1.0	$0.3, 3.0$
n_h	Exponent in hindrance function $H\alpha = 1 - \alpha^{n_h}$	2.0	$1.0, 4.0$
ϕ_0	Base slip-shape factor in $\phi\mathrm{Eo}, \mathrm{Mo}$	1.0	$0.5, 2.0$
f_{ref}	Reference friction factor in f_{eff}	0.02	$0.01, 0.05$
a_f	Nonlinearity parameter in $f_{\mathrm{eff}}\mathrm{Re}_m, \alpha$	0.5	$0.2, 1.0$
μ_{n}	Nominal effective viscosity level	0.05 Pa s	$0.01, 0.2$

Table 3 Representative drift-flux and friction parameters θ that are estimated jointly with influx in the inverse problem. Numerical values illustrate typical prior magnitudes rather than fixed design choices.

Symbol	Interpretation	Dependence	Comment
$c^\star p, T, \chi$	Equilibrium dissolved-gas concentration	p, T, χ	Solves $\Psi p, T, c^\star = 0$
$\Psi p, T, c$	Fugacity residual $\ln f_g - \ln f_l$	p, T, c	Implicit thermodynamic constraint
k_m	Mass-transfer coefficient in $\Gamma = k_m a_i c^\star - c$	Flow regime	Larger in turbulent bubbly flow
a_i	Interfacial area density $a_i = 6\alpha d_b$	α, d_b	Links holdup to transfer rate
d_b	Effective bubble diameter	p, T, α	Encodes coalescence and breakup
β_c	Swelling coefficient in $v_l^{\mathrm{spec}} p, T, c$	c	Couples dissolution to hydrostatics

Table 4 Key quantities in the solubility-constrained thermodynamic closure that governs partitioning between free and dissolved gas.

likelihood ratio computed over a short window:

$$\Lambda = \mathcal{J}_0^\star - \mathcal{J}_1^\star, \quad \mathcal{J}_i^\star = \min_{q,\theta \in \mathcal{M}_i} \mathcal{J} q, \theta, \tag{4.3}$$

where under $\mathcal{M}_0$ the minimization excludes q (or enforces $q = 0$), and under $\mathcal{M}_1$ it includes q with the smoothness prior. Large positive Λ indicates that permitting influx substantially improves the fit after accounting for complexity penalties imposed by priors and regularization. Threshold selection can be based on false-alarm tolerance and can be adapted to time-varying noise levels by scaling with an estimate of R [34].

Because drilling operations are nonstationary, a purely windowed deterministic optimization can be fragile if the window contains unmodeled events such as pump startups. To improve robustness, the framework can be interpreted as a Bayesian filter with augmented state x, θ, q and process noise that allows slow parameter drift. In a Gaussian approximation, an extended Kalman filter or ensemble Kalman filter can propagate mean and covariance, while the differentiable forward model supplies linearizations. In a non-Gaussian setting, a particle filter can represent multimodality arising from ambiguity between dissolution and influx magnitude [35]. The differentiable simulator still plays a central role by enabling proposal distributions informed by gradients rather than random-walk proposals that are inefficient in high dimensions.

A key observability question is whether surface data contain enough information to distinguish influx timing from dissolution storage. The model exposes this through sensitivity analysis. Denote by $S_q t = \partial H \partial q$ the sensitivity of measurements to influx history [36]. When dissolution is strong, S_q can be delayed and smoothed, reducing early detectability. However, the same mechanism introduces sensitivity to solubility parameters χ, creating a trade space: if χ is treated as known, detection may be delayed but characterization may be more stable; if χ is treated as uncertain, the estimator may initially attribute anomalies to χ rather than q unless the data provide discriminatory information, such as simultaneous pressure and temperature deviations. The proposed Bayesian formulation does not remove this fundamental limitation; it makes it explicit by producing posterior uncertainty bands that reflect ambiguity rather than hiding it in ad hoc thresholds.

The practical output of the inference engine is therefore not merely a binary detection flag [37]. It is an evolving posterior distribution over influx rate and cumulative influx volume, along with credible intervals for nuisance parameters

Location / quantity	Condition or relation	Status	Data source
Bottom influx ($z = L$)	$A\alpha\rho_g v_g = m_{\text{in}}t$	Unknown	Inferred boundary flux qt
Circulation rate	$A\rho_m v_m = m_{\text{circ}}t \ m_{\text{in}}t$	Known input	Pump schedule / flow meter
Wellhead pressure ($z = 0$)	$p0, t$ plus choke dynamics	Observed	Wellhead pressure sensor
Pit volume	$V_{\text{pit}} = q_{\text{in}} - q_{\text{out}}$	Observed	Active-pit monitoring
Standpipe pressure	Function of annular and drillstring hydraulics	Observed	Standpipe gauge
Temperature	Tz, t, possibly at selected depths	Optional	DTS / downhole tools

Table 5 Representative boundary conditions and observation channels used to couple the annular model to operational measurements.

Element	Representation in model	Treated as	Time scale
State xt	Discretized fields p, T, v_m, α, c	Dynamic variable	Fast
Influx qt	Time-varying boundary flux at $z = L$	Control to infer	Medium
Parameters θ	Hydraulic, thermal, and solubility coefficients	Slowly varying	Slow
Measurement noise ε	Gaussian with covariance R	Random process	Instantaneous
Bias states	Additive biases on pit volume and pressures	Latent states	Very slow

Table 6 Main components of the state-space formulation underlying the inverse problem for real-time kick characterization.

that influence detection latency. This supports decision-making that is proportional to uncertainty: for example, an operator may choose a conservative response if the posterior probability of nonzero influx exceeds a certain level even if the point estimate is small, particularly in high-risk HPHT regimes where small influx can evolve rapidly.

5. Numerical Implementation and Evaluation Protocol

The coupled thermo-solutal drift-flux equations are stiff because gas compressibility, exsolution, and drift can induce rapid changes in holdup and pressure over short time scales, especially near the surface where pressure is low and expansion is strong. Stiffness is exacerbated in inverse problems because the estimator explores parameter sets that may temporarily produce sharper gradients than the nominal model [38]. The numerical implementation is therefore designed around conservative discretization, implicit time stepping, and solver strategies that preserve differentiability.

Spatial discretization uses a finite-volume method on a mesh $\{z_i\}$ that can align with casing shoes, riser joints, and geometric transitions where Az and $D_h z$ change. Conservative variables are stored as cell averages, and fluxes are computed at faces. To avoid non-differentiable flux limiters, the scheme uses a smooth high-resolution reconstruction based on differentiable blending functions rather than piecewise minmod-type limiters. The goal is not to eliminate numerical diffusion entirely, but to ensure that sensitivity with respect to parameters is stable and that small perturbations in parameters do not cause discontinuous changes in the numerical solution that would derail gradient-based inference [39].

Time integration uses an implicit, variable-step scheme such as backward differentiation. At each step, a nonlinear system is solved for the new state. The Newton method uses analytically assembled Jacobians when possible, with automatic differentiation as a fallback for complex closures. The thermodynamic equilibrium condition for $c^\star$ is solved with a damped Newton iteration embedded inside the outer Newton method, but it is exposed as an implicit function so that derivatives propagate correctly through the equilibrium solve [40]. This nested implicit structure is central: it avoids if-then phase switching and instead treats phase partitioning as a smooth constraint, which is crucial for stable adjoints.

The observation operator H links the downhole state to surface measurements. Wellhead pressure corresponds to $pz = 0, t$ adjusted by choke dynamics if modeled; pit gain is computed from the imbalance between inflow and outflow integrated over time, with outflow linked to mixture superficial velocity and

Model	Assumption on influx qt	Optimized quantities	Typical usage
$\mathcal{M}_0$ (null)	$qt \equiv 0$	θ only	Baseline tracking, false-alarm control
$\mathcal{M}_1$ (influx)	qt free with smoothness prior	q, θ	Kick detection and characterization
Regularized	qt penalized via $q^2 dt$	q, θ	Enforces physically smooth entries
Hybrid	Piecewise-constant segments in qt	Segment heights and θ	Scenario-based studies

Table 7 Detection hypotheses and associated optimization problems used in generalized likelihood-ratio decision statistics.

Aspect	Numerical choice	Motivation
Spatial discretization	Finite-volume scheme on depth-aligned mesh	Conservation and geometric flexibility
Temporal integration	Implicit variable-step method (e.g., BDF)	Stability for stiff thermo-solutal dynamics
Nonlinear solve	Newton iterations with analytic Jacobians	Robust convergence and stable sensitivities
Thermodynamic solve	Nested Newton solve for $\Psi p, T, c^\star = 0$	Smooth phase partitioning without switches
Observation operator	Differentiable mapping Hx, u, θ	Compatible with adjoint-based gradients
Checkpointing	Store selected states for adjoint integration	Limits memory in moving-horizon estimation

Table 8 Key numerical implementation choices for integrating the thermo-solutal drift-flux model and its adjoint in real time.

density at the surface return line. In practice, pit-volume measurements often exhibit drift and quantization; the framework includes an additive bias state with a slow random walk so that the estimator does not misinterpret bias as influx [41]. Similarly, pump-rate measurements can be delayed and noisy; the input channel is therefore modeled with a small lag that can be estimated, improving realism without introducing discontinuities.

Evaluation of an early-detection system requires metrics that reflect operational value rather than purely numerical error. The protocol adopted here emphasizes detection latency, false alarm rate under realistic operational transients, and uncertainty calibration. Detection latency is measured as the time between the onset of influx and the time when the posterior probability of nonzero influx exceeds a threshold, or when the likelihood-ratio statistic exceeds its threshold [42]. False alarms are evaluated under scenarios where pump ramps, heave-induced pressure oscillations, and temperature drifts occur without influx. Uncertainty calibration is assessed by comparing predicted credible intervals for key quantities (such as cumulative influx) with their realized values in synthetic truth models or replayed field events, checking whether, for example, nominal 90% credible intervals contain the truth approximately 90% of the time over an ensemble.

Because field data with labeled ground truth are rare, the framework is designed to support systematic synthetic experiments. A high-fidelity truth model, potentially including richer rheology or multidimensional effects, can generate synthetic measurements that drive the inference engine [43]. The inference engine then operates under model mismatch, which is more realistic than self-consistency tests. Importantly, the purpose of such experiments is not to demonstrate perfect reconstruction, but to characterize failure modes and to identify which sensors improve observability of dissolution versus influx. For instance, adding distributed temperature sensing can significantly reduce ambiguity in solubility capacity, while adding accurate return-flow measurement can sharpen pit-gain dynamics that are otherwise smoothed by tank mixing.

Computational cost is a decisive factor for online deployment [44]. The implicit forward solve is more expensive per step than an explicit scheme, but it permits larger time steps in slow dynamics and prevents instability in stiff regimes. The adjoint solve adds a backward pass comparable in cost to the forward pass. In a moving-horizon setting, warm starts and checkpointing reduce total cost, and reduced-order surrogates

Metric	Definition (schematic)	Interpretation
Detection latency	Time from influx onset to threshold crossing in Λ or posterior $Pq \neq 0$	Speed of kick detection
False-alarm rate	Frequency of detections under $qt \equiv 0$ operational transients	Spurious-trigger probability
Posterior coverage	Fraction of cases where true influx lies in nominal credible interval	Calibration of uncertainty bands
Computational cost	Wall-clock time per unit simulated time	Suitability for online deployment
Robustness to mismatch	Sensitivity of estimates to model simplifications and parameter errors	Reliability under field conditions

Table 9 Illustrative metrics used to evaluate the performance of the proposed inference framework in synthetic and replayed scenarios.

can be used selectively. A practical strategy is to maintain the full model for estimation but to precompute local reduced bases for sensitivity exploration, using operator inference to approximate the Jacobian actions required by the Newton and adjoint iterations [45]. The surrogate is not used as a black-box replacement; it is used as a preconditioner and as a proposal generator in probabilistic filters, preserving physical constraints while accelerating convergence.

Robustness also depends on parameterization choices. If too many parameters are allowed to vary freely, the inverse problem becomes ill posed and the estimator may fit noise. If too few parameters are allowed, model mismatch may be absorbed into influx estimates, increasing false alarms [46]. The Bayesian framework provides a compromise: parameters are allowed to vary but are penalized by priors whose strength reflects confidence. In operational contexts, these priors can be updated offline using calibration data from known transients, then held fixed online. This separation between offline calibration and online inference reduces computational burden and mitigates identifiability issues.

Finally, although the model is one-dimensional, it is structured to admit systematic extensions [47]. For instance, annular eccentricity and cuttings loading can be introduced through effective area and friction surrogates that depend on measured torque and drag signals, while still preserving differentiability. Likewise, simple heave models can be included as boundary perturbations, allowing the estimator to attribute periodic pressure variations to heave rather than influx. The emphasis remains on mechanisms that matter for detection and that can be constrained by available data.

6. Conclusion

This paper presented a differentiable, thermo-solutal drift-flux inference framework aimed at real-time gas-kick detection and characterization from sparse surface measurements [48]. The central idea is to treat the kick as an unknown boundary influx to be inferred jointly with uncertain hydraulic, thermal, and mass-transfer parameters, while maintaining thermodynamic consistency between free gas and dissolved inventory so that dissolution-induced delays and muted surface indicators are modeled explicitly rather than absorbed into bias. The governing equations were formulated in conservative form with drift-flux kinematics, coupled to an implicit thermodynamic equilibrium constraint and finite-rate mass transfer that together define a smooth partitioning of gas mass between phases. By using implicit discretization and discrete-adjoint sensitivities, the approach enables gradient-based posterior updates whose computational cost scales favorably with the dimension of the inferred influx history, supporting moving-horizon estimation and likelihood-ratio detection statistics.

The framework emphasizes uncertainty quantification and identifiability [49]. It makes explicit the ambiguity between small influx and strong dissolution capacity and shows how multi-sensor fusion and thermodynamic coupling can reduce that ambiguity when temperature and pressure information are available. Numerical implementation considerations were discussed with a focus on stiffness, differentiability, and robustness under model mismatch, including conservative finite-volume discretization, implicit solvers with consistent Jacobians, and the use of reduced-order surrogates as accelerators rather than black-box replacements.

While the model remains one-dimensional, its differentiable, constraint-based structure provides a practical backbone for kick-aware automation: it can be extended to incorporate additional operational effects and calibrated offline while delivering online probabilistic estimates of influx and associated uncertainty. The principal outcome is a unified modeling-and-inference approach that links mechanistic multiphase physics to statistically grounded detection decisions under realistic operational uncertainty [50].

Acknowledgments

We would like to thank the reviewers of this research for their helpful comments and suggestions.

References

[1] S. Rassenfoss, “More exact measures raise tough questions: Regulators and drillers adjust to precise fluid flow measures,” *Journal of Petroleum Technology*, vol. 67, pp. 50–53, 8 2015.

[2] J. Feng, J. Fu, P. Chen, and L. Xu, “Investigation of

methane/drilling mud phase behavior and its influence to hydrocarbon drilling activity," *Energy Science & Engineering*, vol. 7, pp. 1280–1291, 4 2019.

[3] A. K. Sleiti, G. Takalkar, M. H. El-Naas, A. R. Hasan, and M. A. Rahman, "Early gas kick detection in vertical wells via transient multiphase flow modelling: A review," *Journal of Natural Gas Science and Engineering*, vol. 80, p. 103391, 2020.

[4] L. Mao, M. Cai, Q. Liu, and G. Wang, "Dynamical simulation of high-pressure gas kick in ultra-deepwater riserless drilling," *Journal of Energy Resources Technology*, vol. 143, pp. 1–31, 10 2020.

[5] M. Prakasha, "Evaluasi perencanaanpressurized mud cap drillingdengan pengaruh viskositas pada annular fluidterhadap gas migration velocity pada sumur xlapangan y," 3 2015.

[6] W. E. S. Vielma, R. Quijada, D. Feltracco, V. Mittiga, I. Mosti, and K. Nergaard, "Increasing drilling operational margins of an onshore mature field in pakistan by including a dynamic drilling modeling approach," *SPE Europec featured at 79th EAGE Conference and Exhibition*, 6 2017.

[7] R. Guo, Y. Chen, R. P. Coutinho, and P. J. Waltrich, "Numerical and experimental investigations of gas kick migration during casing while drilling," in *SPE Health, Safety, Security, Environment, & Social Responsibility Conference - North America*, SPE, 4 2017.

[8] L. Neto and E. Gonzaga, "Comportamento pvt de misturas de dióxido de carbono em emulsões base n-parafina," 2 2014.

[9] C. Baumann, D. Gultom, H. Williams, A. Yudhatama, and R. Rahman, "Wireline perforating technology maximizes well productivity and minimizes operational risks," in *SPE Latin America and Caribbean Petroleum Engineering Conference*, SPE, 5 2014.

[10] J. Schubert, "Technology focus: Well control (january 2011)," *Journal of Petroleum Technology*, vol. 63, pp. 70–70, 1 2011.

[11] L. Jolly and J. Woods, "A new dawn for mandated fuel-ethanol programmes: separating fact from fiction.," *International Sugar Journal*, vol. 106, pp. 118–125, 8 2004.

[12] D. Dupuis and S. Hancock, "Ad equation between a second generation semi and drilling extended-reach well in tunisia," *IADC/SPE Drilling Conference*, 3 2008.

[13] I. Sagala and M. Tingay, "Analysis of overpressure and its generating mechanisms in the northern carnarvon basin from drilling data," *The APPEA Journal*, vol. 52, pp. 375–390, 6 2012.

[14] A. Ababila, "Evaluasi penanggulangan well kick dengan metode driller pada sumur eksplorasi "neb" lapangan "jb"pt. petrochina international jabung ltd," 5 2018.

[15] P. F. Hopkins, D. Kereš, N. Murray, E. Quataert, and L. Hernquist, "Stellar feedback & bulge formation in clumpy disks," *Monthly Notices of the Royal Astronomical Society*, vol. 427, pp. 968–978, 11 2012.

[16] K. Manikonda, A. R. Hasan, O. Kaldirim, J. J. Schubert, and M. A. Rahman, "Understanding gas kick behavior in water and oil-based drilling fluids," in *SPE Kuwait oil and gas show and conference*, p. D043S023R001, SPE, 2019.

[17] "Good to go? assessing the environmental performance of new mobility," 9 2020.

[18] G. Schurman, "An improved procedure for handling a threatened blowout," *Journal of Petroleum Technology*, vol. 18, pp. 437–444, 4 1966.

[19] D. C. Marques, P. Ribeiro, O. L. A. Santos, and R. F. T. Lomba, "Thermodynamic behavior of olefin and methane mixtures applied to synthetic drilling fluids well control," in *SPE Latin America and Caribbean Petroleum Engineering Conference*, SPE, 5 2017.

[20] M. Zulqarnain and M. Tyagi, "Quantitative risk assessment (qra) of an exploratory drilling oil spill in deepwater gulf of mexico," in *Volume 5: Materials Technology; Petroleum Technology*, American Society of Mechanical Engineers, 6 2014.

[21] K. Bybee, "Drilling underbalanced from a drillship in the santos basin," *Journal of Petroleum Technology*, vol. 58, pp. 74–76, 4 2006.

[22] "Triplets become wide binaries," *Astronomy & Geophysics*, vol. 54, pp. 1.8–a–1.8, 1 2013.

[23] D. Veeningen, "Detect kicks prompted by losses and direct measurement well control method through networked drill-string with along string pressure evaluation," *SPE/IADC Drilling Conference*, 3 2013.

[24] Z. Ma, A. K. Vajargah, A. Ambrus, P. Ashok, D. Chen, E. van Oort, R. May, J. D. Macpherson, G. Becker, and D. A. Curry, "Multi-phase well control analysis during managed pressure drilling operations," in *SPE Annual Technical Conference and Exhibition*, SPE, 9 2016.

[25] K. Manikonda, A. R. Hasan, A. Barooah, N. H. Rahmani, M. El-Naas, A. K. Sleiti, and M. A. Rahman, "A mechanistic gas kick model to simulate gas in a riser with water and synthetic-based drilling fluid," in *Abu Dhabi International Petroleum Exhibition and Conference*, p. D012S116R009, SPE, 2020.

[26] P. Qin, A. Andreanov, H. C. Park, and S. Flach, "Interacting ultracold atomic kicked rotors: loss of dynamical localization," *Scientific reports*, vol. 7, pp. 41139–41139, 1 2017.

[27] N. Taryana, "Perhitungan kecepatan gelombang akustik refleksi dalam analisa performansi sumur minyak menggunakan well analyzer echometer berbasis total well management (twm)," 11 2016.

[28] M. I. Goldman, "The dog barks but the caravan moves on," *Demokratizatsiya: The Journal of Post-Soviet Democratization*, vol. 15, pp. 360–370, 9 2007.

[29] M. Yu, A. K. Vajargah, S. Z. Miska, R. Majidi, and M. E. Ozbayoglu, "Taking the proper action to gas influx during constant bottom-hole pressure technique of managed pressure drilling," in *Offshore Technology Conference*, OTC, 5 2013.

[30] M. Ledenko, "Razmatranja kontrole tlaka u podvodnom bušenju," 9 2017.

[31] F. Shanks, D. Hammett, and H. Zinkgraf, "Experience drilling in deepwater high current areas," in *Offshore Technology Conference*, OTC, 4 1979.

[32] I. Sule, F. Khan, and S. Butt, "Experimental investigation of gas kick effects on dynamic drilling parameters," *Journal of Petroleum Exploration and Production Technology*, vol. 9, pp. 605–616, 6 2018.

[33] A. A. Azizov, W. Davila, S. S. Janwadkar, J. A. Fabian, R. Fortelney, and B. Welch, "Optimized steerable motor design overcomes drilling challenges in the fayetteville shale unconventional play," in *SPE Middle East Unconventional Gas Conference and Exhibition*, SPE, 1 2012.

[34] Y. W. Hong and R. van Kuilenburg, "Active mud line pumping, design, testing and future possibilities in rig design," in *IADC/SPE Drilling Conference and Exhibition*, SPE, 3 2018.

[35] P. O'bryan, "Well control problems associated with gas solubility in oil-based drilling fluids.," 1 1988.

[36] M. Stanislawek, "Analysis of alternative well control methods for dual density deepwater drilling," 11 2004.

[37] J. Xie, B. Yu, X. Zhang, Q. Shao, and X. Song, "Numerical simulation of gas-liquid-solid three-phase flow in deep wells," *Advances in Mechanical Engineering*, vol. 5, pp. 951298–, 1 2013.

[38] A. Dutta, M. A. Hosani, J. A. Aranda, R. Masoud, A. I. Jaiyeola, M. A. Baslaib, A. M. A. Bairaq, A. M. A. Hammadi, M. Ahmad, V. Radman, and A. E. Shahat, "Effective multilateral open hole sidetrack strategy in thin reservoir units for maximum reservoir contact-a case study of onshore drilling in uae," in *Abu Dhabi International Petroleum Exhibition & Conference*, SPE, 11 2019.

[39] M. J. Graham, K. E. S. Ford, B. McKernan, N. P. Ross, D. Stern, K. B. Burdge, M. W. Coughlin, S. G. Djorgovski, A. J. Drake, D. A. Duev, M. M. Kasliwal, A. Mahabal, S. van Velzen, J. Belecki, E. C. Bellm, R. Burruss, S. B. Cenko, V. Cunningham, G. Helou, S. R. Kulkarni, F. J. Masci, T. A. Prince, D. J. Reiley, H. Rodriguez, B. Rusholme, R. Smith, and M. T. Soumagnac, "Candidate electromagnetic counterpart to the binary black hole merger gravitational wave event s190521g," *Physical review letters*, vol. 124, pp. 251102–, 6 2020.

[40] T. M. Bryant, D. S. Grosso, and S. N. Wallace, "Gas-influx detection with mwd technology," *SPE Drilling Engineering*, vol. 6, pp. 273–278, 12 1991.

[41] B. Patel, T. D. Cooper, S. Hughes, and W. C. Billings, "The application of advanced gas analysis system complements early kick detection and control capabilities of mpd with added hse value," in *SPE/IADC Managed Pressure Drilling and Underbalanced Operations Conference and Exhibition*, SPE, 3 2012.

[42] J. Marklof, "Kinetic limits of dynamical systems," 8 2014.

[43] K. R. Krishnamurthy, "Slipstream pilot-scale demonstration of a novel amine-based post-combustion technology for carbon dioxide capture from coal-fired power plant flue gas," 2 2017.

[44] G. R. Darmawan, N. B. Sangka, S. D. Susilo, J. T. Shaun, S. W. Nas, A. E. Prasetia, and S. Sisworo, "Integrated downhole isolation valve and managed pressure drilling to facilitate development of sour fractured-limestone gas reservoir in east java, indonesia," *SPE/IADC Drilling Conference and Exhibition*, 3 2011.

[45] J. Hofmann, D. Fusselman, and R. Liles, "New source air pollution permits in texas and new mexico," in *Permian Basin Oil and Gas Recovery Conference*, SPE, 3 1994.

[46] L. Sala, E. Cenci, P. R. Capelo, A. Lupi, and M. Dotti, "Non-isotropic feedback from accreting spinning black holes," *Monthly Notices of the Royal Astronomical Society*, vol. 500, pp. 4788–4800, 11 2020.

[47] O. Weustink, "Bombax 48-inch pipeline installation," in *Offshore Technology Conference*, OTC, 5 2003.

[48] O. G. Steine, R. Rommetveit, and T. Harris, "Full scale kick detection system testing relevant for slim-hole/hpht drilling," *SPE Annual Technical Conference and Exhibition*, pp. 13–28, 10 1995.

[49] E. Vefring, R. Rommetveit, and E. Borge, "An advanced kick simulator operating in a user-friendly x-window system environment," in *Petroleum Computer Conference*, SPE, 6 1991.

[50] S. M. Willson, A. S. Nagoo, and M. M. Sharma, "Analysis of potential bridging scenarios during blowout events," *SPE/IADC Drilling Conference*, pp. 345–363, 3 2013.